Early Hominin Foot Morphology Based on 1.5-Million-Year-Old Footprints from Ileret, Kenya

Matthew R. Bennett, *et al.*

Science **323**, 1197 (2009);
DOI: 10.1126/science.1168132

when approaching the HOMO or LUMO resonance of the molecular wire (*28*). The increased conductance at higher bias voltages then compensates for the molecular wire length increase in Fig. 4B (a factor of 40 is not sufficient for the achieved current increase). Thus, such a setup allows the determination of the small conductance (8.6×10^{-13} S) of a single and the same molecular wire with 20 nm length (the conductance at small bias voltages cannot be measured over such a large distance, due to the extremely low current—below the detection limit—passing through the polymer in this case). In this regard, it would be interesting to prepare and study conjugated polymers with smaller HOMO-LUMO gaps. Such molecular wires should exhibit higher conductances and allow charge transport to be determined over even larger distances.

References and Notes

1. C. Joachim, J. K. Gimzewski, A. Aviram, *Nature* **408**, 541 (2000).
2. A. Nitzan, *Annu. Rev. Phys. Chem.* **52**, 681 (2001).
3. A. Nitzan, M. A. Ratner, *Science* **300**, 1384 (2003).
4. N. J. Tao, *Nat. Nanotechnol.* **1**, 173 (2006).
5. C. Joachim, J. K. Gimzewski, R. R. Schlittler, C. Chavy, *Phys. Rev. Lett.* **74**, 2102 (1995).
6. M. A. Reed, C. Zhou, C. J. Muller, T. P. Burgin, J. M. Tour, *Science* **278**, 252 (1997).
7. R. M. H. Smit *et al.*, *Nature* **419**, 906 (2002).
8. J. Reichert *et al.*, *Phys. Rev. Lett.* **88**, 176804 (2002).
9. S. Wu *et al.*, *Nat. Nanotechnol.* **3**, 569 (2008).
10. M. Kiguchi *et al.*, *Phys. Rev. Lett.* **101**, 046801 (2008).
11. B. Xu, N. J. Tao, *Science* **301**, 1221 (2003).
12. W. Haiss *et al.*, *J. Am. Chem. Soc.* **125**, 15294 (2003).
13. X. Xiao, B. Xu, N. Tao, *J. Am. Chem. Soc.* **126**, 5370 (2004).
14. J. He *et al.*, *J. Am. Chem. Soc.* **127**, 1384 (2005).
15. S. H. Choi, B. Kim, C. D. Frisbie, *Science* **320**, 1482 (2008).
16. W. Haiss *et al.*, *Nat. Mater.* **5**, 995 (2006).
17. R. Temirov, A. Lassise, F. B. Anders, F. S. Tautz, *Nanotechnology* **19**, 065401 (2008).
18. F. Kühner, M. Erdmann, H. E. Gaub, *Phys. Rev. Lett.* **97**, 218301 (2006).
19. S. K. Kufer, E. M. Puchner, H. Gumpp, T. Liedl, H. E. Gaub, *Science* **319**, 594 (2008).
20. T. Zambelli *et al.*, *Int. J. Nanoscience* **3**, 331 (2004).
21. L. Grill *et al.*, *Nat. Nanotechnol.* **2**, 687 (2007).
22. Materials and methods are available as supporting material on *Science* Online.
23. L. Limot, J. Kröger, R. Berndt, A. Garcia-Lekue, W. A. Hofer, *Phys. Rev. Lett.* **94**, 126102 (2005).
24. C. Joachim, M. A. Ratner, *Proc. Natl. Acad. Sci. U.S.A.* **102**, 8801 (2005).
25. M. Magoga, C. Joachim, *Phys. Rev. B* **56**, 4722 (1997).
26. M. Magoga, C. Joachim, *Phys. Rev. B* **57**, 1820 (1998).
27. D. Neher, *Macromol. Rapid Commun.* **22**, 1365 (2001).
28. C. Joachim, M. Magoga, *Chem. Phys.* **281**, 347 (2002).

29. Financial support from the European Integrated Project PICO INSIDE and the Deutsche Forschungsgemeinschaft (DFG) through SFB 658 and contract GR 2697/1-2 is gratefully acknowledged.

Supporting Online Material

www.sciencemag.org/cgi/content/full/323/5918/1193/DC1
Materials and Methods
Figs. S1 to S6
References

10 November 2008; accepted 16 January 2009
10.1126/science.1168255

Early Hominin Foot Morphology Based on 1.5-Million-Year-Old Footprints from Ileret, Kenya

Matthew R. Bennett,[1]* John W.K. Harris,[2] Brian G. Richmond,[3,4] David R. Braun,[5] Emma Mbua,[6] Purity Kiura,[6] Daniel Olago,[7] Mzalendo Kibunjia,[6] Christine Omuombo,[7] Anna K. Behrensmeyer,[8] David Huddart,[9] Silvia Gonzalez[9]

Hominin footprints offer evidence about gait and foot shape, but their scarcity, combined with an inadequate hominin fossil record, hampers research on the evolution of the human gait. Here, we report hominin footprints in two sedimentary layers dated at 1.51 to 1.53 million years ago (Ma) at Ileret, Kenya, providing the oldest evidence of an essentially modern human–like foot anatomy, with a relatively adducted hallux, medial longitudinal arch, and medial weight transfer before push-off. The size of the Ileret footprints is consistent with stature and body mass estimates for *Homo ergaster/erectus*, and these prints are also morphologically distinct from the 3.75-million-year-old footprints at Laetoli, Tanzania. The Ileret prints show that by 1.5 Ma, hominins had evolved an essentially modern human foot function and style of bipedal locomotion.

Bipedalism is a key human adaptation that appears in the fossil record by 6 million years ago (Ma) (*1*). Considerable debate continues over when and in what context a modern human–like form of bipedalism evolved, because of a fragmentary record and disagreements over the functional interpretations of existing fossils and footprints (*2*–*7*). Modern human footprints reflect the specialized anatomy and function of the human foot, which is characterized by a fully adducted hallux, a large and robust calcaneus and tarsal region, a pronounced medial longitudinal arch, and short toes (*2*). Footprints reflect the pressure distribution as the foot makes contact with the substrate, but also the sediment's geomechanical properties (*8*). During normal walking, the weight-bearing foot undergoes a highly stereotypical movement and pressure distribution pattern in which the heel contacts the ground first, making a relatively deep impression on the substrate. This is followed by contact with the lateral side of the foot and metatarsal heads, after which weight transfers to the ball of the foot with peak pressure under the medial metatarsal heads, and finally ending with toe-off pressure under the hallux (*9*, *10*). As a consequence, the deepest part of a footprint often occurs beneath the first and second metatarsal heads, that along with a deep hallucal impression corresponds to the peak pressures at toe-off (*10*). The extent to which any pressure, or footprint impression, occurs medially varies with the anatomy of the midfoot, including the height of the longitudinal arch and other factors (*11*), and the extent to which lateral toes leave impressions depends on factors such as foot orientation relative to the direction of travel, transverse versus oblique push-off axes, and substrate properties. This contrasts with the less stereotypical pattern of footfall observed in African apes during quadrupedal and bipedal locomotion. Here the heel and lateral mid-foot make contact with the ground first, followed by contact with the lateral toes that are often curled and with a hallux that is often widely abducted. Lift-off in the African apes is variable, but it usually involves relatively low pressure during final contact by both the lateral toes and widely abducted hallux, in stark contrast to modern human foot function (*11*).

Here, we report hominin footprints from the Okote Member of the Koobi Fora Formation (*12*), second in age only to the mid-Pliocene (3.7 Ma) Laetoli prints (*13*), located close to Ileret, Kenya (Fig. 1; site FwJj14E; latitude 4°18′44″N, longitude 36°16′16″E). The footprints are found in association with animal prints on two stratigraphically separated levels and were digitized with an optical laser scanner (Fig. 1) (*14*). The upper surface contains three hominin footprint trails comprising two trails of two prints and one of seven prints, as well as a number of isolated prints (Figs. 2 and 3 and figs. S3 and S6 to S11). The lower surface, approximately 5 m below, preserves one trail of two prints and a single isolated hominin print (Fig. 3). The footprints occur within a 9-m-thick sequence of fine-grained, normally

[1]School of Conservation Sciences, Bournemouth University, Poole, BH12 5BB, UK. [2]Department of Anthropology, Rutgers University, 131 George Street, New Brunswick, NJ 08901, USA. [3]Center for the Advanced Study of Hominid Paleobiology, Department of Anthropology, George Washington University, Washington, DC 20052, USA. [4]Human Origins Program, National Museum of Natural History, Smithsonian Institution, Washington, DC 20013–7012, USA. [5]Department of Archaeology, University of Cape Town, Private Bag, Rondebosch 7701, South Africa. [6]National Museums of Kenya, Post Office Box 40658-00100, Nairobi, Kenya. [7]Department of Geology, University of Nairobi, Post Office Box 30197, Nairobi, Kenya. [8]Department of Paleobiology, MRC 121, National Museum of Natural History, Smithsonian Institution, Washington, DC, 20013–7012, USA. [9]School of Biological and Earth Sciences, Liverpool John Moores University, Liverpool, L3 3AF, UK

*To whom correspondence should be addressed. E-mail: mbennett@bmth.ac.uk

graded, silt and sand units deposited as overbank flood deposits with evidence of paleosol development. Interbedded within this succession are three fluvially reworked volcanic ashes; the upper ash (Northern Ileret Tuff) forms a prominent landscape bench that correlates with other nearby sites where traces of hominin activity have been recovered (*15*) and is unconformably overlain by the Galana Boi Formation of Holocene age (*12*). The ash layers are correlated geochemically to dated tuffs within the Turkana Basin, thereby providing an age of 1.51 to 1.52 Ma for the upper tuff and 1.53 Ma for the lower tuff (Fig. 1) (*14*, *16*).

The prints from both the upper and lower levels at FwJj14E have a well-defined, deeply depressed and adducted hallux; visible lateral toe impressions that vary in depth of indentation; a well-defined ball beneath the first and second metatarsal heads; and a visible instep reflecting a medial longitudinal arch. The angle of hallux abduction, relative to the long axis of the foot, is typically 14° compared to, and statistically distinct from (table S4), 8° for the modern reference prints and 27° for the Laetoli prints (Fig. 4A). The morphology of the Ileret prints suggests that the feet of these hominins had functional medial longitudinal arches. In prints FUT1-2 and FLI1, for example, the medial side of the mid-print is slightly raised, indicating a lack of substrate impression in this area (Figs. 2 and 3). A comparison of the instep width relative to the width in the metatarsal head region shows that the upper prints at FwJj14E fall within the modern human range and are distinct from the relatively wider insteps characterizing the Laetoli prints (Fig. 4C). The FwJj14E lower prints show more variability; the two prints that differ from modern human prints appear to have undergone taphonomic mediolateral compression (fig. S13). Most of the Ileret prints are similar in length to the longest modern human prints (fig. S19), although the isolated footprint on the lower level (FLI1; Fig. 3) is significantly smaller, despite a similar gross anatomy, and may represent a subadult.

The contours of the upper- and lower-level FwJj14E prints suggest a modern human–like toe-off mechanism, in contrast to the more ambiguous evidence from the Laetoli footprints

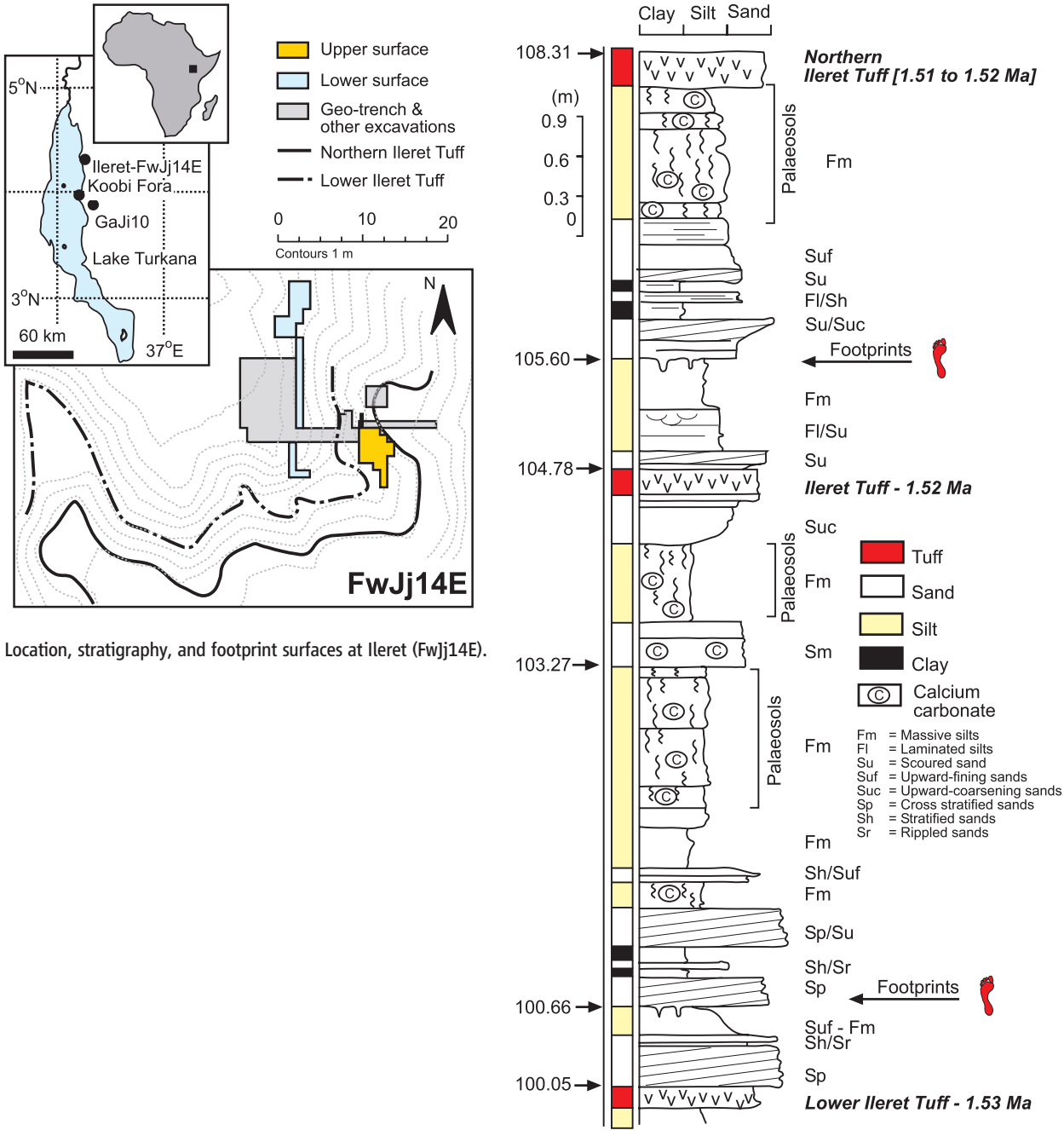

Fig. 1. Location, stratigraphy, and footprint surfaces at Ileret (FwJj14E).

(Fig. 4B). Both the upper and lower Ileret prints show the greatest depth in the metatarsal head region to be typically medially located, in contrast to its lateral position in many of the Laetoli prints (fig. S19). In the majority of the modern human prints, the normal shift in pressure from lateral to medial in late stance phase, with peak medial pressures, is registered in the greater medial depth. However, the variability shows that fully modern feet during walking can also produce prints with greater lateral depth (fig. S19) (*3*, *6*), demonstrating variability in the foot function, something that is further complicated by the geomechanical properties of the substrate. Therefore, a laterally concentrated depth cannot, in itself, rule out (for instance, in the Laetoli prints) a foot structure capable of medial weight transfer in late stance phase. However, the modern human–like relative instep width (Fig. 4C) and medially concentrated ball impression in the Ileret prints provide compelling positive evidence of a medial longitudinal arch and the medial pressure shift and push-off from the ball of the foot beneath the medial metatarsal heads.

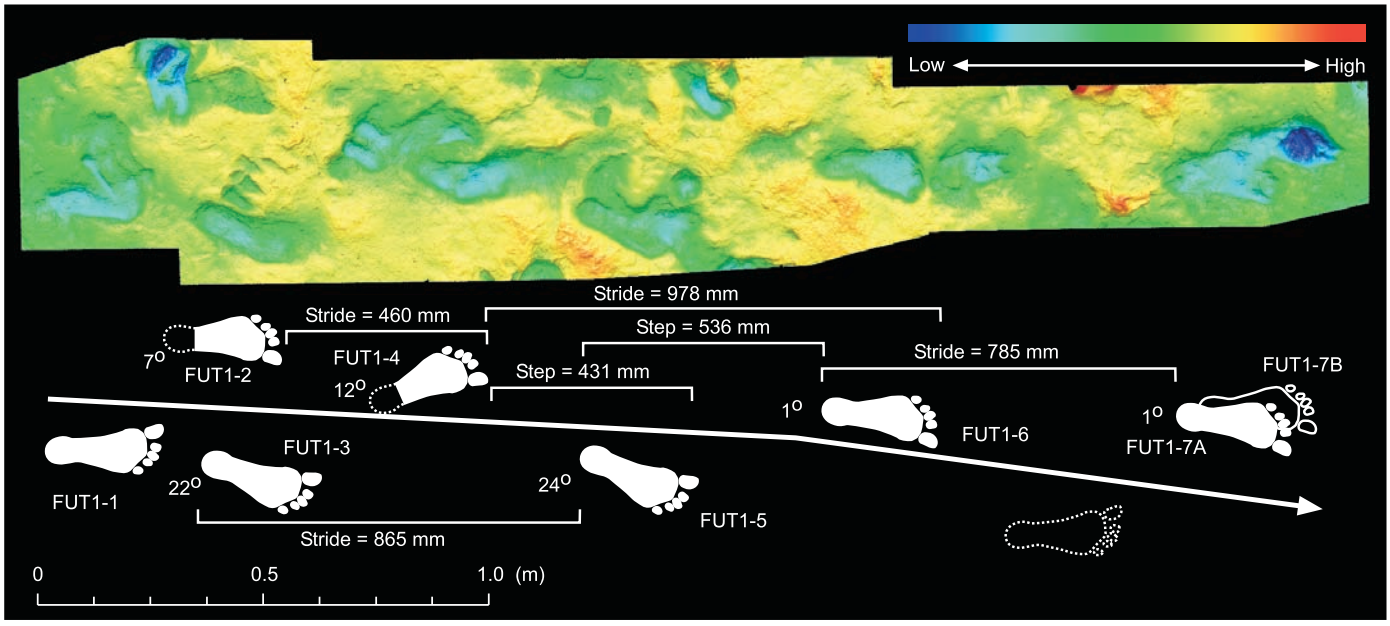

Fig. 2. Tessellated swath of optical laser scans of the main footprint trail on the upper footprint surface at FwJj14E. Color is rendered with 5-mm isopleths.

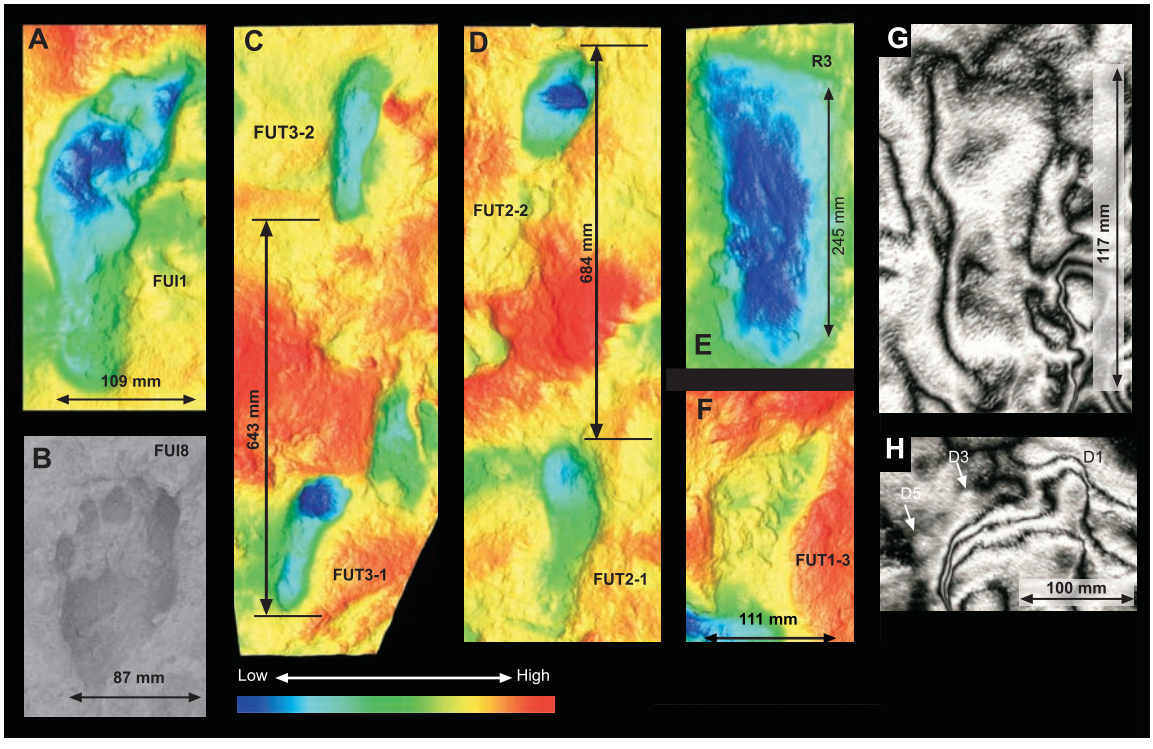

Fig. 3. Optical laser scan images color-rendered with 5-mm isopleths for footprints at both FwJj14E and GaJi10. (**A**) Isolated left foot (FUI1) on the upper footprint surface at FwJj14E. (**B**) Photograph of FUI8 on the upper footprint surface at FwJj14E, showing good definition of the toe pads; the second toe is partially obscured by the third toe. (**C**) Second trail on the upper footprint surface at FwJj14E, showing two left feet. (**D**) Third trail on the upper footprint surface at FwJj14E, showing a right and a left foot. (**E**) Print R3 from GaJi10 (*22*), re-excavated and scanned as part of this investigation. (**F**) Partial print (FUT1-2) on the upper footprint surface at FwJj14E; the heel area has been removed by a later bovid print. (**G**) Print FLI1 on the lower footprint surface at FwJj14E, rendered with 5-mm alternating black and white isopleths. (**H**) Inverted image of the toe area of print FUT1-1 with alternating 5-mm black and white isopleths. Note the locations of the pads of the small toes and the presence of a well-defined ball beneath the hallucial metatarsophalangeal joint. The first, third, and fifth toes are marked D1, D3, and D5, respectively.

These are hallmarks of modern human walking that can be related to a long stride with extended lower limbs, key to the energetic efficiency of human walking (*17*).

Inferences about stride are possible from the short trails at FwJj14E. The longest trail (FUT1) consists of seven prints, initially with three closely spaced prints suggesting an individual either standing with feet astride or who slowed before walking forward with an increasing step length (Fig. 2). Typical stride lengths vary from 460 to 785 mm, with step lengths in the range of 431 to 536 mm in the direction of travel; foot angles vary, but are typically parallel to the direction of travel, diverging by 1° to 24°. Using the average of the last three strides (average = 876 mm) and a hip height of 860 mm estimated from foot length (258 mm, the average of the four clearest prints of the FUT1 trail), we estimate a velocity of approximately 0.63 m/s (*14*). This is a slow speed consistent with someone beginning to walk from a standing (or slowed) position and the variability in step lengths may attest to the challenges of walking on an uneven muddy surface already marred by a range of animal prints. Although precise foot-to-stature ratios are unknown for early Pleistocene hominins, we use as a rough estimate ones developed for Australian Aborigines (*18*) and Kenyan Dassenach (*14*), on the basis that their statures are adapted for a semiarid environment. Using this relationship, we estimate the average height of the individuals from the prints on the upper surface to be 1.75 ± 0.26 m and 1.76 ± 0.26 m for those on the lower surface, excluding the potential subadult (print FUI1) which gives a height of 0.92 ± 0.13 m (table S2). The large stature and mass estimates derived from the Ileret prints compare well with those of *Homo ergaster/erectus* on the basis of postcranial remains and are significantly larger than postcrania-based stature and mass estimates for *Paranthropus boisei* and *Homo habilis* (table S3) (*19*–*21*), suggesting that the prints at FwJj14E were made by *Homo ergaster/erectus* individuals.

Behrensmeyer and Laporte (*22*) reported hominin footprints at site GaJi10 (latitude 3°44′15″N, longitude 36°55′48″E), 45 km to the south of FwJj14E, in 1981. The footprint surface occurs below a prominent tuff, sampled and correlated here to the Akait Tuff, dated to 1.435

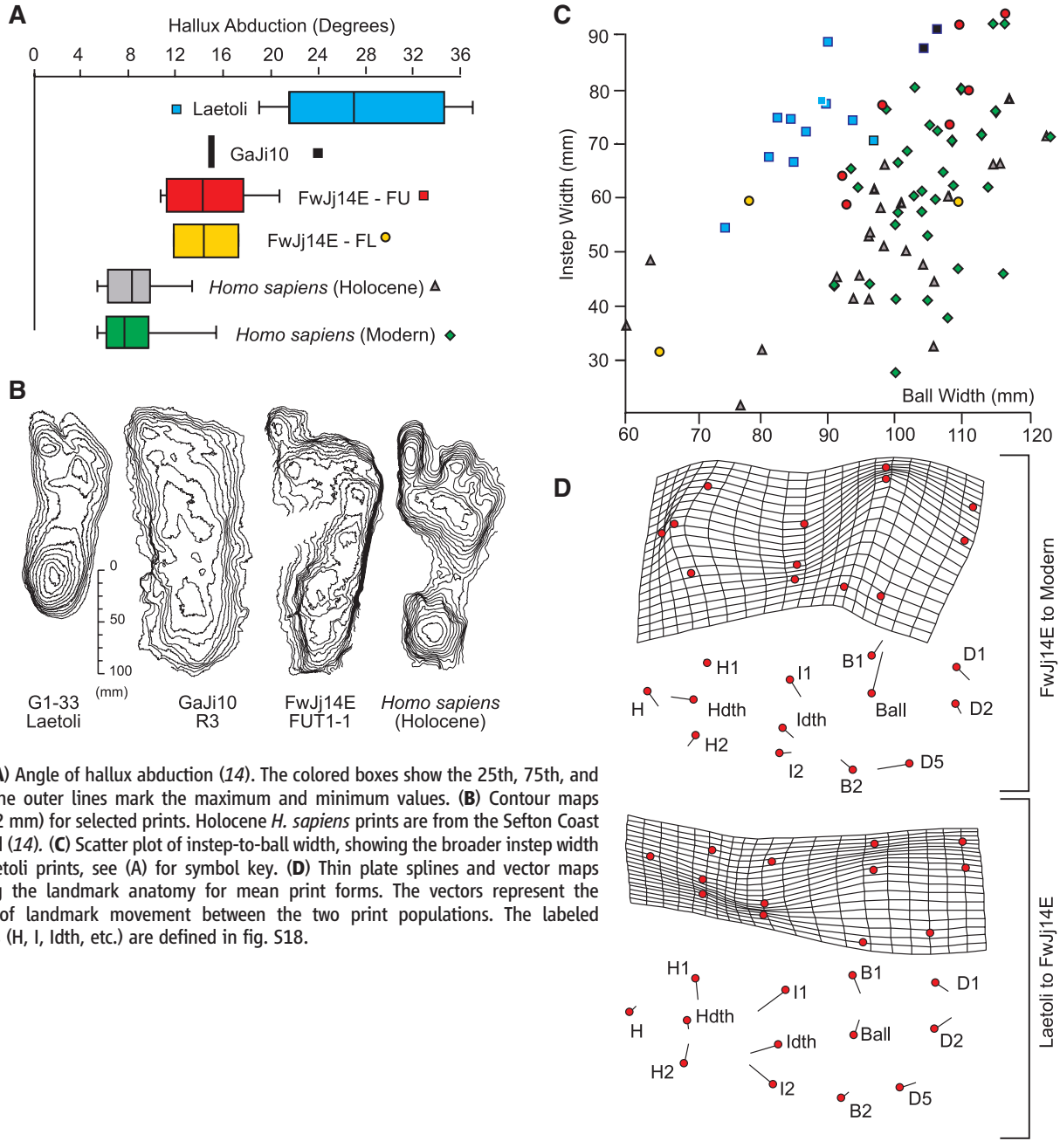

Fig. 4. (**A**) Angle of hallux abduction (*14*). The colored boxes show the 25th, 75th, and median; the outer lines mark the maximum and minimum values. (**B**) Contour maps (interval, 2 mm) for selected prints. Holocene *H. sapiens* prints are from the Sefton Coast in England (*14*). (**C**) Scatter plot of instep-to-ball width, showing the broader instep width of the Laetoli prints, see (A) for symbol key. (**D**) Thin plate splines and vector maps comparing the landmark anatomy for mean print forms. The vectors represent the direction of landmark movement between the two print populations. The labeled landmarks (H, I, Idth, etc.) are defined in fig. S18.

Ma (*14*). Re-excavation of these prints uncovered four of the original seven prints and a new print, and the two best-preserved examples are comparable to those at FwJj14E (*14*).

To further evaluate the morphology of the prints at FwJj14E and compare them objectively with samples of modern human and Laetoli footprints, we digitized 13 landmarks on each footprint scan and used generalized Procrustes analysis to compare their shapes (*14*). Figure 4D shows thin plate splines and landmark vector maps comparing the mean landmark positions (in two dimensions) of the Ileret prints with the modern human and Laetoli prints (*14*). When the prints from the two levels at FwJj14E are compared, both surfaces show similar anatomical differences from the modern prints, with a narrower heel and ball area and a wider instep associated with less pronounced arch elevation (Fig. 4D and fig. S20). When compared to the Laetoli prints, the Ileret prints have a more contracted proximal mid-foot region, including a deeper instep (Fig. 4D), suggesting the presence of a medial longitudinal arch. The location of the narrowest point of the instep also lies farther forward (more distal) in the Laetoli prints than in both the modern and Ileret prints, possibly reflecting differences in foot proportions or a lack of definition of the instep. Discriminant analysis was also used to compare the different print populations (*14*); 8 of the 10 prints at FwJj14E used in the analysis were classified with modern prints and two with Laetoli prints (table S6).

The Ileret footprints show the earliest evidence of a relatively modern human–like foot with an adducted hallux, a medial longitudinal arch, and medial weight transfer before push-off. Although we cannot conclude with certainty what hominin species made the footprints at FwJj14E or GaJi10, these modern human characteristics, in combination with the large size of the prints, are most consistent with the large size and tall stature evident in some *Homo ergaster/erectus* individuals (*19*, *20*). These prints add to the anatomical (*19*, *20*, *23*) and archaeological (*24*, *25*) evidence pointing to a major transition in human evolution with the appearance of hominins with long lower limbs, conferring advantages at a lower energetic cost (*26*), and archaeological indications of activities in a variety of ecological settings and the transport of resources over long distances (*27*). These lines of evidence, together with the earliest evidence of a relatively modern foot anatomy and function, support the hypothesis that this was a hominin with a larger home range related to increasing average body size and enhanced dietary quality (*28*). These factors add to an emerging picture of the paleobiology of *H. ergaster/erectus* that suggests a shift in cultural and biological adaptations relative to earlier hominins.

References and Notes

1. B. G. Richmond, W. L. Jungers, *Science* **319**, 1662 (2008).
2. N. L. Griffin, B. Wood, in *The Human Foot: A Companion to Clinical Studies*, L. Klenerman, B. Wood, Eds. (Springer-Verlag, London, 2006), pp. 27–79.
3. T. D. White, G. Suwa, *Am. J. Phys. Anthropol.* **72**, 485 (1987).
4. R. H. Tuttle, D. Webb, E. Weidle, M. Baksh, *J. Arch. Sci.* **17**, 347 (1990).
5. J. Charteris, J. J. Wall, J. W. Nottrodt, *Am. J. Phys. Anthropol.* **58**, 133 (1982).
6. D. J. Meldrum, in *From Biped to Strider: The Emergence of Modern Human Walking, Running, and Resource Transport*, D. J. Meldrum, C. E. Hilton, Eds. (Kluwer Academic/Plenum Publishers, New York, 2004), pp. 63–83.
7. J. T. Stern Jr., R. L. Susman, *Am. J. Phys. Anthropol.* **60**, 279 (1983).
8. J. R. L. Allen, *Philos. Trans. R. Soc. London Ser. B* **352**, 481 (1997).
9. H. Elftman, J. Manter, *Am. J. Phys. Anthropol.* **20**, 69 (1935).
10. E. Vereecke, K. D'Aout, D. De Clercq, L. Van Elsacker, P. Aerts, *Am. J. Phys. Anthropol.* **120**, 373 (2003).
11. E. Morag, P. R. Cavanagh, *J. Biomech.* **32**, 359 (1999).
12. C. S. Feibel, F. H. Brown, I. McDougall, *Am. J. Phys. Anthropol.* **78**, 595 (1989).
13. M. D. Leakey, R. L. Hay, *Nature* **278**, 317 (1979).
14. Materials and methods, additional illustrations, statistical analysis, and discussion of tuff geochemistry at FwJj14E are available as supporting material on *Science* Online.
15. J. W. K. Harris, D. G. Braun, J. T. McCoy, B. L. Pobiner, M. J. Rogers, *J. Hum. Evol.* **42**, A15 (2002).
16. F. H. Brown, B. Haileab, I. McDougall, *J. Geol. Soc. London* **163**, 185 (2006).
17. M. D. Sockol, D. A. Raichlen, H. Pontzer, *Proc. Natl. Acad. Sci. U.S.A.* **104**, 12265 (2007).
18. S. Webb, M. L. Cupper, R. Robins, *J. Hum. Evol.* **50**, 405 (2006).
19. C. B. Ruff, A. Walker, in *The Nariokotome* Homo erectus *Skeleton*, A. C. Walker, R. E. F. Leakey, Eds. (Harvard Univ. Press, Cambridge, MA, 1993), pp. 234–265.
20. H. M. McHenry, K. Coffing, *Annu. Rev. Anthropol.* **29**, 125 (2000).
21. F. Spoor *et al.*, *Nature* **448**, 688 (2007).
22. A. K. Behrensmeyer, L. F. Laporte, *Nature* **289**, 167 (1981).
23. B. G. Richmond, L. C. Aiello, B. A. Wood, *J. Hum. Evol.* **43**, 529 (2002).
24. M. J. Rogers, J. W. K. Harris, C. S. Feibel, *J. Hum. Evol.* **27**, 139 (1994).
25. B. L. Pobiner, M. J. Rogers, C. M. Monahan, J. W. K. Harris, *J. Hum. Evol.* **55**, 103 (2008).
26. H. Pontzer, *J. Exp. Biol.* **210**, 1752 (2007).
27. D. R. Braun, J. W. K. Harris, D. N. Maina, *Archaeometry* 10.1111/j.1475-4754.2008.00399 (2008).
28. S. C. Antón, W. R. Leonard, M. L. Robertson, *J. Hum. Evol.* **43**, 773 (2002).

29. This project is part of the Koobi Fora Research and Training Program, which is jointly run by the National Museum of Kenya and Rutgers University and supported by the Holt Family Foundation, M. Weiss, B. Mortenson, G. Noland, C. Chip, and the Wenner-Gren Foundation for Anthropological Research. B. Wood provided valuable comments on a draft of the paper, and the dating was undertaken by F. Brown. The field assistance of H. Manley, S. A. Morse, and M. J. Steele is acknowledged.

Supporting Online Material

www.sciencemag.org/cgi/content/full/323/5918/1197/DC1
Methods
SOM Text
Figs. S1 to S22
Tables S1 to S6
References and Notes

5 November 2008; accepted 19 January 2009
10.1126/science.1168132

RNA Polymerase IV Functions in Paramutation in *Zea mays*

Karl F. Erhard Jr., Jennifer L. Stonaker,* Susan E. Parkinson,* Jana P. Lim, Christopher J. Hale, Jay B. Hollick†

Plants have distinct RNA polymerase complexes (Pol IV and Pol V) with largely unknown roles in maintaining small RNA–associated gene silencing. Curiously, the eudicot *Arabidopsis thaliana* is not affected when either function is lost. By use of mutation selection and positional cloning, we showed that the largest subunit of the presumed maize Pol IV is involved in paramutation, an inherited epigenetic change facilitated by an interaction between two alleles, as well as normal maize development. Bioinformatics analyses and nuclear run-on transcription assays indicate that Pol IV does not engage in the efficient RNA synthesis typical of the three major eukaryotic DNA-dependent RNA polymerases. These results indicate that Pol IV employs abnormal RNA polymerase activities to achieve genome-wide silencing and that its absence affects both maize development and heritable epigenetic changes.

In maize, mouse, and other eukaryotes, paramutation refers to a process by which heritable changes in gene regulation are facilitated by interactions between alleles on homologous chromosomes (*1*). As typically described, alleles conferring relatively high gene action invariably change to a repressed expression state when heterozygous with specific alleles or allelic states (*1*). Operationally, paramutation violates the first law of Mendelian inheritance that alleles segregate unchanged from a heterozygote and thus has important implications for normal genome function and evolution (*2*, *3*), though few examples have proved experimentally tractable.

In maize, paramutations occurring at the *Pl1-Rhoades* (*Pl1-Rh*) allele of the *purple plant 1* (*pl1*) locus involve at least four genes (*4*–*6*), two of which appear to be part of a small interfering RNA (siRNA) heterochromatin pathway (*7*–*9*). Repressed expression states of *Pl1-Rh* resulting from

Department of Plant and Microbial Biology, 111 Koshland Hall, University of California, Berkeley, CA 94720-3102, USA.

*These authors contributed equally to this work.
†To whom correspondence should be addressed. E-mail: hollick@nature.berkeley.edu